APPLIED SCIENCES AND ENGINEERING

A probiotic nanozyme hydrogel regulates vaginal microenvironment for *Candida* vaginitis therapy

Gen Wei[1], Quanyi Liu[1,2,3], Xiaoyu Wang[1], Zijun Zhou[1], Xiaozhi Zhao[4], Wanqing Zhou[5], Wanling Liu[1], Yihong Zhang[1], Shujie Liu[1], Chenxin Zhu[1], Hui Wei[1,6]*

Molecular therapeutics are limited for *Candida* vaginitis because they damage normal cells and tissues of vagina, aggravating the imbalance of vaginal microbiota and increasing the recurrence. To tackle this limitation, through the combination of peroxidase-like rGO@FeS_2 nanozymes [reduced graphene oxide (rGO)] with *Lactobacillus*-produced lactic acid and H_2O_2, a responsive hyaluronic acid (HA) hydrogel rGO@FeS_2/*Lactobacillus*@HA (FeLab) is developed. FeLab has simultaneous anti–*Candida albicans* and vaginal microbiota–modulating activities. In particular, the hydroxyl radical produced from rGO@FeS_2 nanozymes and *Lactobacillus* kills *C. albicans* isolated from clinical specimens without affecting *Lactobacillus*. In mice with *Candida* vaginitis, FeLab has obvious anti–*C. albicans* activity but hardly damages vaginal mucosa cells, which is beneficial to vaginal mucosa repair. Moreover, a higher proportion of *Firmicutes* (especially *Lactobacillus*) and a decrease in *Proteobacteria* reshape a healthy vaginal microbiota to reduce the recurrence. These results provide a combined therapeutic of nanozymes and probiotics with translational promise for *Candida* vaginitis therapy.

INTRODUCTION

Candida vaginitis, a common fungal vulvovaginal inflammatory disease usually caused by *Candida albicans* (*1*), occurs in approximately 75% of all women worldwide. Even more seriously, 5 to 8% of these women have suffered from recurrence. Because of its high incidence and nature of recurrence, *Candida* vaginitis affects both the physical and mental health of women (*2*, *3*). Pathologically, vaginal microbiota plays a key role in maintaining the vaginal microenvironment and health (*4*). In particular, *Lactobacillus* is the dominant beneficial bacterium (*5*). It maintains the balance of vaginal microbiota, which protects the vagina from foreign microorganisms by producing lactic acid and antibacterial substances, forming a biological barrier, and protecting vaginal epithelial cells (*6*, *7*).

Recently, the probiotic therapy has attracted great research interest partially because the current *Candida* vaginitis therapy is not satisfactory (*8*, *9*). There are four most widely deployed antifungal drugs to treat *Candida* vaginitis, including Clotrimazole, Fluconazole, Miconazole, and Nystatin (*10*). However, some of them only halt the growth of fungi but do not kill them (*11*). Moreover, their long-term use can cause certain damage to the normal cells and tissues of vagina, which will further aggravate local vaginal microbiota imbalance, acid-base balance disorder, superinfection, and recurrence, thus greatly increasing the difficulty of clinical treatments (*12*). Therefore, it is urgent to explore *Candida* vaginitis therapies that can modulate the vaginal microenvironment.

Because of its dominance in healthy vaginal microbiota, *Lactobacillus* has been explored to develop probiotic *Candida* vaginitis therapies (*9*, *13*). While *Lactobacillus* preparations have great potential in treating and preventing bacterial vaginitis, the therapeutic effect on *Candida* vaginitis is not satisfactory (*8*, *14*, *15*). A possible explanation is that *C. albicans* is a eukaryotic cell with mycelium and spores, which are more tolerant; while *Lactobacillus* generates some antibacterial substances, such as H_2O_2, lactic acid, and bacteriocin, which are too mild to kill *C. albicans* (*16*, *17*). We reason that converting mild H_2O_2 to more toxic hydroxyl radical ($^{\bullet}OH$) would be a promising therapeutic strategy.

$^{\bullet}OH$ can be generated from H_2O_2 through metal ion–mediated Fenton reactions (such as Fe^{2+}) or enzyme-mediated catalysis (such as myeloperoxidase–nicotinamide adenine dinucleotide) (*18*, *19*). Nevertheless, the metal ions for Fenton reactions can be detrimental to normal cells and tissues (*20*). On the other hand, enzymes are unstable and immunogenic, limiting their practical applications. Encouragingly, nanozymes (the functional nanomaterials with enzyme-like properties) have shown a promising capability to produce reactive oxygen species (ROS), including $^{\bullet}OH$, for biomedical applications (*21*–*23*). Recent studies have shown that some peroxidase (POD)–like nanozymes can produce $^{\bullet}OH$ and exhibit high antimicrobial activities (*24*). Here, by taking advantage of the complementary merits of POD-like nanozymes and probiotic *Lactobacillus*, we developed a responsive hyaluronic acid (HA) hydrogel-rGO@FeS_2 [reduced graphene oxide (rGO)]/*Lactobacillus*@HA (designated as FeLab) to effectively treat *Candida* vaginitis and reduce the recurrence. When applied into the vagina, the hyaluronidase (HAase) secreted by *C. albicans* and bacteria can degrade HA (*25*), thereby locally releasing *Lactobacillus* and rGO@FeS_2 nanozymes. On the one hand, *Lactobacillus* ferments and generates lactic acid to normalize the vaginal microenvironment and reduce vaginal pH to 4 to 4.5 (*7*). On the other hand, the rGO@FeS_2 nanozymes can catalyze *Lactobacillus*-produced H_2O_2 to generate a large

[1]Department of Biomedical Engineering, College of Engineering and Applied Sciences, Nanjing National Laboratory of Microstructures, Jiangsu Key Laboratory of Artificial Functional Materials, Nanjing University, Nanjing, Jiangsu 210023, China. [2]State Key Laboratory of Electroanalytical Chemistry, Changchun Institute of Applied Chemistry, Chinese Academy of Sciences, Changchun, Jilin 130022, China. [3]University of Science and Technology of China, Hefei, Anhui 230026, China. [4]Department of Andrology, Nanjing Drum Tower Hospital, the Affiliated Hospital of Nanjing University Medical School, Nanjing, Jiangsu 210008, China. [5]Department of Clinical Laboratory, Nanjing Drum Tower Hospital, The Affiliated Hospital of Nanjing University Medical School, Nanjing, Jiangsu 210008, China. [6]State Key Laboratory of Analytical Chemistry for Life Science, School of Chemistry and Chemical Engineering, Chemistry and Biomedicine Innovation Center (ChemBIC), Nanjing University, Nanjing, Jiangsu 210023, China.
*Corresponding author. Email: weihui@nju.edu.cn

amount of ˙OH, killing *C. albicans* (Fig. 1). Notably, our system not only inhibited the clinical isolates but also exhibited satisfactory therapeutic efficacy for *C. albicans*–induced vaginitis in vivo. Moreover, compared with clinical drugs, our system is much friendlier to the vagina and can reduce the recurrence. Therefore, we implemented a promising strategy to treat and reduce the recurrence of *Candida* vaginitis by simultaneously regulating the vaginal microenvironment and catalyzing the killing of *C. albicans*.

RESULTS

Characterization of rGO@FeS_2 nanozymes

Previous studies demonstrated that Fe-N-rGO with Fe^{2+} exhibited excellent POD-like activity because it had an optimal adsorption energy for OH (*26*, *27*). Therefore, in this work, we chose marcasite FeS_2 nanoparticles with POD-like activity after our preliminary screening study. Compared with several other iron-containing nanozymes [i.e., Pt_3Fe, Fe_3O_4, and pyrite FeS_2 nanozymes (*28*–*30*)] (figs. S1 and S2), the rGO@FeS_2 nanozymes with H_2O_2 generated the most amount of ˙OH, which was captured by 5,5-dimethyl-1-pyrroline *N*-oxide (DMPO) and analyzed by electron paramagnetic resonance (EPR) (fig. S3). rGO was used to stabilize marcasite FeS_2 nanoparticles. Otherwise, marcasite FeS_2 nanoparticles would easily aggregate, preventing the biomedical applications (*31*, *32*). As shown via transmission electron microscopy (TEM) imaging, rGO had a two-dimensional lamellar structure (Fig. 2A), and marcasite FeS_2 nanoparticles were evenly distributed on the surface of rGO (Fig. 2B). In contrast, marcasite FeS_2 nanoparticles alone aggregated obviously (Fig. 2C). In addition, the high-angle annular dark-field scanning TEM (HAADF-STEM) and corresponding elemental mapping images (fig. S4) showed the even presence of C, N, Fe, and S elements without obvious large aggregates of marcasite FeS_2 nanoparticles. These results showed the importance of rGO as the supports to stabilize and improve the dispersity of marcasite FeS_2 nanoparticles. Furthermore, a lattice spacing of 0.24 nm corresponding to the (111) plane of marcasite FeS_2 was identified by high-resolution TEM imaging (fig. S5) (*33*). Meanwhile, the crystalline feature of rGO@FeS_2 was studied. As shown in Fig. 2D, the characteristic peaks in the x-ray diffraction (XRD) patterns were indexed to rGO and the cubic phase of marcasite FeS_2 (Joint Committee on Powder Diffraction Standards (JCPDS) card number 74-1051) (*30*, *34*). Then, we analyzed the surface chemical compositions and electronic states by x-ray spectroscopy (XPS). The XPS survey spectrum (Fig. 2E) showed typical peaks of C 1*s*, N 1*s*, O 1*s*, Fe 2*p*, and S 2*p*. The high-resolution C 1*s* XPS spectrum showed the presence of C═C/C─C, C─O/C─N, and C═O at 284.6, 285.7, and 287.1 eV, respectively (fig. S6A). The N 1*s* XPS spectrum could be deconvoluted into three peaks at 398.2, 400.1,

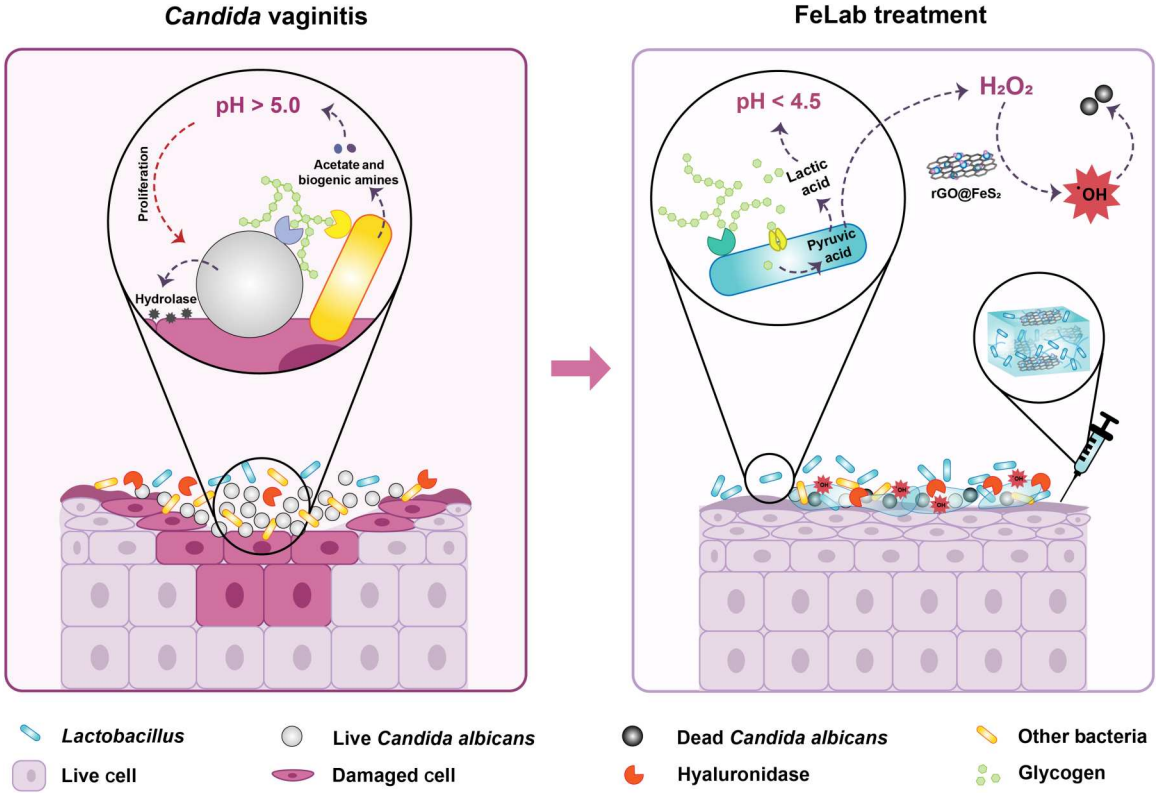

Fig. 1. Schematic illustrating *Candida* vaginitis microenvironment and FeLab-enabled microenvironmental regulation for *Candida* vaginitis therapy. Left: *Candida* vaginitis microenvironment characterized with hyperproliferating *C. albicans*, elevated vaginal pH, imbalance of vaginal microbiota, and damaged vaginal mucosal cells. **Right:** FeLab-enabled microenvironmental regulation for *Candida* vaginitis therapy. The HAase secreted by *C. albicans* and bacteria can degrade HA, which releases *Lactobacillus* and rGO@FeS_2 nanozymes. Subsequently, released *Lactobacillus* ferments and generates lactic acid to normalize the vaginal microenvironment and reduce vaginal pH to 4 to 4.5. Simultaneously, the released rGO@FeS_2 nanozymes can catalyze *Lactobacillus*-produced H_2O_2 to generate a large amount of ˙OH, killing *C. albicans*.

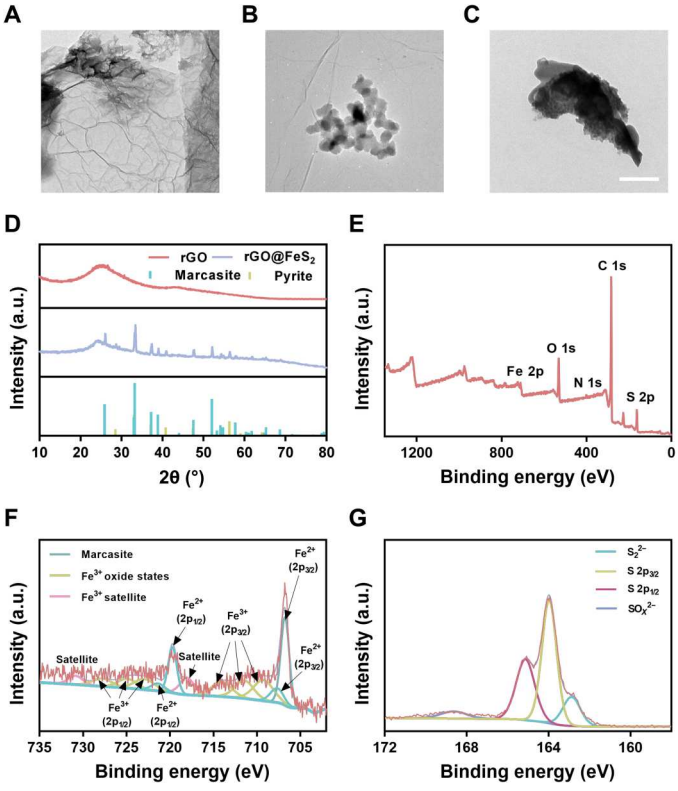

Fig. 2. Characterization of rGO@FeS_2 nanozymes. (**A** to **C**) TEM images of rGO (A), rGO@FeS_2 (B), and marcasite FeS_2 (C), respectively. Scale bar, 200 nm. (**D**) XRD patterns of rGO and rGO@FeS_2. The lines at the bottom mark the reference patterns of marcasite FeS_2 (JCPDS card number 74-1051) and pyrite FeS_2 (JCPDS card number 42-1340). a.u., arbitrary units. (**E**) XPS spectrum of rGO@FeS_2. (**F** and **G**) XPS spectra for Fe 2*p* (F) and S 2*p* (G) regions of rGO@FeS_2.

and 402.8 eV (fig. S6B), which corresponded to pyridinic N, pyrrolic N, and oxidized N. For Fe 2*p*, the representative peaks of marcasite FeS_2 nanoparticles, originating from electron deficiency of Fe^{2+} created by the breaking of Fe—S bonds, were around 707.4 eV (Fe $2p_{3/2}$) and 720.5 eV (Fe $2p_{1/2}$), respectively. Moreover, there were several peaks at 710 to 715 eV and 724 to 728 eV, which could be assigned to Fe^{3+} oxide states due to the precursor $FeCl_3$ and slight oxidation of marcasite FeS_2 in air (Fig. 2f). The S 2*p* peaks located at 162.8, 163.9, and 165.1 eV were attributed to S_2^{2-}, S $2p_{3/2}$, and S $2p_{1/2}$, respectively. In addition, another SO_x^{2-}-related peak at 168.3 eV was correlated with the inevitable oxidation of marcasite FeS_2 (Fig. 2G) (*33*, *35*). These binding energies of both S 2*p* and Fe 2*p* were consistent with those in marcasite FeS_2. The above results showed the successful synthesis of rGO@FeS_2 nanozymes.

POD-like and anti–*C. albicans* activities of rGO@FeS_2 nanozymes

We used the oxidation of 3,3′,5,5′-tetramethylbenzidine (TMB) in the presence of H_2O_2 to examine the POD-like activity of rGO@FeS_2 nanozymes. As shown in Fig. 3A, only the system containing rGO@FeS_2 nanozymes, H_2O_2, and TMB turned blue [the color of oxidized TMB (oxTMB)]. The corresponding absorption spectrum of the system exhibited a strong absorption peak at 652 nm, suggesting that rGO@FeS_2 nanozymes had a strong POD-like activity. Moreover, the POD-like activity of rGO@FeS_2 nanozymes was pH dependent. Figure 3B shows that rGO@FeS_2 nanozymes exhibited a stronger POD-like activity under acidic conditions and had an optimal activity at pH 4 to 4.5. In addition, enzymatic kinetics analysis of rGO@FeS_2 nanozymes toward H_2O_2 and TMB substrates was performed. For comparison, other iron-containing nanozymes (i.e., Pt_3Fe, Pyrite FeS_2, and Fe_3O_4) were also investigated. Both the Michaelis-Menten constant (K_m) and maximum initial velocity (v_{max}) were obtained (figs. S7 and S8 and table S1). We further analyzed the relationship between the kinetics parameters and anti–*C. albicans* activity among these four nanozymes. As shown in fig. S9, there was no direct correlation between the anti–*C. albicans* activities and the kinetics parameters of these four POD-like nanozymes.

Next, we used EPR spectroscopy to investigate the $^{\bullet}OH$ generating activity of rGO@FeS_2 nanozymes, which would be critical for the anti–*C. albicans* therapy. As shown in Fig. 3C, rGO@FeS_2 nanozymes can effectively catalyze a low concentration of H_2O_2 (80 μM) to generate strong $^{\bullet}OH$. Then, we investigated the anti–*C. albicans* activity of rGO@FeS_2 nanozymes in the presence of H_2O_2 in acetate–sodium acetate buffer solution (HAc-NaAc; pH 5.0) using the colony-forming unit (CFU) method. Compared with other groups, fungal colonies obviously decreased, indicating the lowest survival rate of *C. albicans* in the group treated with both rGO@FeS_2 nanozymes and H_2O_2 (Fig. 3, D and E).

Under the same iron content, the intensity of $^{\bullet}OH$ generation by rGO@FeS_2, Pt_3Fe, Fe_3O_4, and pyrite FeS_2 nanozymes with H_2O_2 showed a positive correlation with their anti–*C. albicans* activities (fig. S10). It was mentioned that the rGO@FeS_2 nanozymes with H_2O_2 had the most notable anti–*C. albicans* activity (figs. S11 and S12), which further highlighted the advantages of rGO@FeS_2 nanozymes. Together, rGO@FeS_2 nanozymes had excellent anti–*C. albicans* activity based on the POD-like activity to generate toxic $^{\bullet}OH$ under acidic conditions, implying great potential for treating *Candida* vaginitis.

rGO@FeS_2 nanozymes with *Lactobacillus* enhanced anti–*C. albicans* activities, including five samples of clinical isolates in vitro

As demonstrated above, H_2O_2 is required and a low pH is preferred for the POD-like activity of rGO@FeS_2 nanozymes. Therefore, we investigated whether the introduction of *Lactobacillus* would produce enough H_2O_2 and lower the pH substantially for rGO@FeS_2 nanozymes to exert POD-like activity in treating *C. albicans* vaginitis. First, we detected the amounts of H_2O_2 generated during the *Lactobacillus* fermentation using a hydrogen peroxide assay kit and drew a standard curve of H_2O_2 accordingly (fig. S13A). As shown in Fig. 4A and fig. S13B, no matter how long it was cultured, *C. albicans* alone did not generate H_2O_2. In contrast, the *Lactobacillus* group generated H_2O_2 in a time-dependent manner, and the highest amount of H_2O_2 was obtained at 36 hours (about 50 μM). Moreover, the cofermentation of *Lactobacillus* with *C. albicans* (i.e., the mixed-species group) also generated H_2O_2. At the optimal cofermentation time (i.e., 24 hours), about 30 μM H_2O_2 was produced, which was lower than that of *Lactobacillus* alone and attributed to nutrient competition between them (*16*). Then, we examined whether *Lactobacillus* could lower the pH of de Man, Rogosa, and Sharpe (MRS) medium. Figure S13C shows that compared with *C. albicans* alone, the mixed-species group

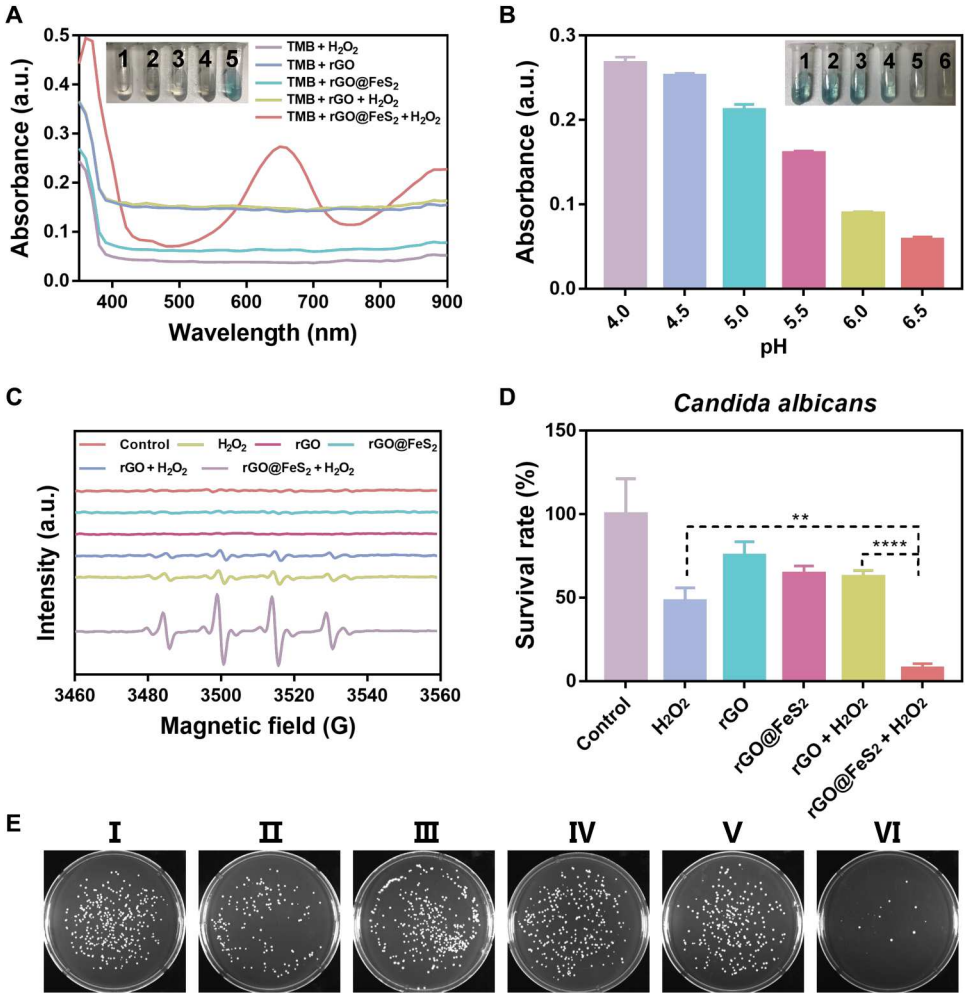

Fig. 3. POD-like and anti–*C. albicans* activities of rGO@FeS_2 nanozymes. (**A**) Ultraviolet-visible absorption spectra and corresponding color changes of TMB in different reaction systems: 1, TMB + H_2O_2; 2, TMB + rGO; 3, TMB + rGO@FeS_2; 4, TMB + rGO + H_2O_2; 5, TMB + rGO@FeS_2 + H_2O_2 in a pH 4.5 HAc-NaAc buffer after 15 min of incubation. (**B**) pH-dependent POD-like activities of rGO@FeS_2. The pH values of insets 1 to 6 are 4.0, 4.5, 5.0, 5.5, 6.0, and 6.5. (**C**) EPR monitoring the generation of $^{\bullet}OH$ by rGO@FeS_2 in the presence of H_2O_2 in a pH 4.5 HAc-NaAc buffer after 5 min of incubation. (**D**) Antifungal effects of rGO@FeS_2 and H_2O_2 on *C. albicans*. (**E**) Digital images of *C. albicans* colonies after different treatments. I to VI correspond to the *x* coordinate of (D), respectively. An 80 μM amount of H_2O_2, rGO, and rGO@FeS_2 at 25 μg/ml was used for anti–*C. albicans* at 37°C for 120 min. Data are presented as means ± SD (n = 3). $^{**}P < 0.01$ and $^{****}P < 0.0001$.

lowered the pH of MRS medium from 5.7 to 4.5 after 24 hours of cofermentation and maintained the pH thereafter. Further studies showed that rGO and rGO@FeS_2 with *Lactobacillus* also lowered the pH of MRS medium (fig. S14). These results indicated that *Lactobacillus* can produce H_2O_2 and lower the pH of MRS medium, the two key requirements to achieve effective probiotic therapy of *Candida* vaginitis. Note that the cofermentation time of 24 hours was optimal and used in the following studies.

Because the cofermentation of *Lactobacillus* with *C. albicans* can generate about 30 μM H_2O_2 (Fig. 4A), we also investigated the anti–*C. albicans* activity of rGO@FeS_2 in the presence of H_2O_2 (30 μM). As shown in fig. S15, compared with other groups, fungal liabilities, and colonies decreased in the rGO@FeS_2 + H_2O_2–treated group, indicating that rGO@FeS_2 nanozymes with a lower concentration of H_2O_2 were still effective for anti–*C. albicans* activity. Then, we studied the anti–*C. albicans* activity of rGO@FeS_2 and *Lactobacillus*. The colony morphology of *C. albicans* and *Lactobacillus* is different. The former grows into large and milky colonies, and the latter forms small and transparent colonies (fig. S16). These morphological characteristics enable us to distinguish them easily, facilitating the study of anti–*C. albicans* activity. As shown in figs. S16 and S17A, the treatment with *Lactobacillus* alone showed a negligible anti–*C. albicans* effect, whereas the treatment with rGO@FeS_2 nanozymes and *Lactobacillus* resulted in a 70% reduction in the viability of *C. albicans*. In addition, rGO, rGO@FeS_2, and rGO with *Lactobacillus* had minimal effects on the viability of *C. albicans*. Moreover, the treatments with rGO/*Lactobacillus* or rGO@FeS_2/*Lactobacillus* hardly affected the viability of *Lactobacillus* (fig. S17B), which may be attributed to certain oxidative stress tolerance of *Lactobacillus* given its H_2O_2 producing property or proliferation and fermentation abilities under microaerophilic conditions (*7*).

To assess the anti–*C. albicans* mechanism of rGO@FeS_2 and *Lactobacillus*, we investigated the oxidative state and structural integrity

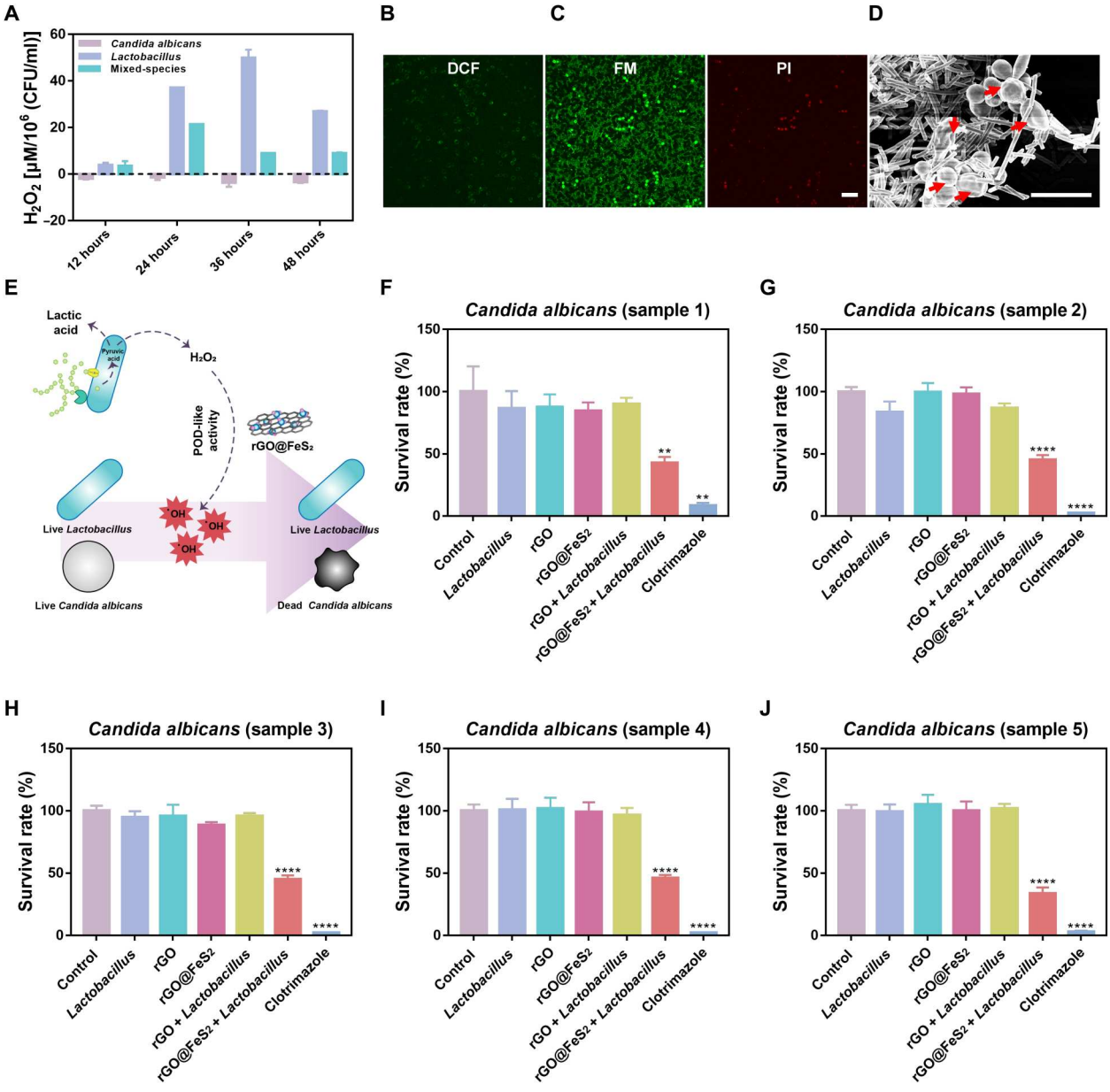

Fig. 4. rGO@FeS_2 nanozymes with *Lactobacillus* enhanced anti–*C. albicans* activities, including five samples of clinical isolates in vitro. (**A**) Amount of H_2O_2 in *C. albicans*, *Lactobacillus*, and mixed-species (*C. albicans* and *Lactobacillus*) groups. (**B** to **D**) ROS level (DCF) (B), cell viability staining (FM and PI) (C), and SEM images (D) of *C. albicans* treated with rGO@FeS_2 nanozymes and *Lactobacillus*. Red arrows show the damaged cells. Scale bars, 20 μm (C) and 10 μm (D). (**E**) Schematic diagram of rGO@FeS_2 catalyzing the generation of $^{\bullet}OH$ from H_2O_2 and lactic acid produced by *Lactobacillus* to kill *C. albicans*. (**F** to **J**) Five different samples of *C. albicans* isolated from clinics treated with the indicated treatments. The medium was MRS medium, and the culture conditions were microaerophilic. The concentration of rGO, rGO@FeS_2, and Clotrimazole was 25 μg/ml. The coincubation time was 24 hours. Data are presented as means ± SD (n = 3). $^{**}P < 0.01$ and $^{****}P < 0.0001$.

of both *C. albicans* and *Lactobacillus*. The intracellular ROS was detected by using 2′,7′-dichlorodihydrofluorescein diacetate (DCFH-DA) as a fluorescence probe. DCFH-DA can be converted to 2′,7′-dichlorofluorescein (DCF) after reacting with ROS. The observation of laser scanning confocal microscopy clearly confirmed that rGO@FeS_2 nanozymes and *Lactobacillus* treatment exhibited the strongest ability to generate intracellular ROS of *C. albicans* compared with other treatments (Fig. 4B and fig. S18A). Moreover, the disruption of *C. albicans* was further demonstrated using green fluorescent plasma membrane and vesiculation dye (FilmTracer FM 1-43) and red fluorescent propidium iodide (PI) nucleic acid dye. FilmTracer FM 1-43 is membrane-permeant, whereas PI only penetrates damaged cell membranes. As shown in Fig. 4C and fig. S18B, the confocal fluorescence images showed the most serious damage to *C. albicans* cell membrane in the group treated with rGO@FeS_2 nanozymes and *Lactobacillus*. In addition, compared with other treatments, characterization of *C. albicans* and *Lactobacillus* surfaces by scanning electron microscope (SEM)

imaging showed that the structural integrity of treated *C. albicans* was the most severely affected after the treatment with rGO@FeS_2 nanozymes and *Lactobacillus* (Fig. 4D and fig. S18C). The oxidative state and structural integrity induced by the treatment of rGO@FeS_2 nanozymes and *Lactobacillus* were observed only on *C. albicans* but not on *Lactobacillus* (Fig. 4, B to D). Collectively, these results demonstrated that rGO@FeS_2 nanozymes can use H_2O_2 and lactic acid produced by *Lactobacillus* to exert POD-like activity and further generate ROS, thereby causing the death of *C. albicans* without affecting the activity of *Lactobacillus*. The corresponding schematic illustration of the self-cascade reaction between rGO@FeS_2 nanozymes and *Lactobacillus* is depicted in Fig. 4E. In general, the combination of rGO@FeS_2 nanozymes and *Lactobacillus* had great potential for treating vaginitis caused by *C. albicans*.

On the basis of the results above, to further demonstrate the translational potential of the self-cascade action between rGO@FeS_2 nanozymes and *Lactobacillus* in the treatment of *Candida* vaginitis, we explored the effects on clinically isolated *C. albicans*, which were named samples 1, 2, 3, 4, and 5, respectively. Similar to the findings in figs. S14, S16, and S17, compared with *Lactobacillus* treatment, the cell viability and colonies of clinically isolated *C. albicans* treated with rGO@FeS_2 nanozymes and *Lactobacillus* were significantly decreased (Fig. 4, F to J and fig. S19). Likewise, the pH of MRS medium could be lowered to around 4.5, and the activities of *Lactobacillus* were hardly affected after the treatment of rGO@FeS_2 nanozymes and *Lactobacillus* (figs. S20 and S21). Meanwhile, we chose Clotrimazole suppository, one of the most commonly used medications in clinics (*10*), for a comparative study of the anti–*C. albicans* activity toward clinical isolates. As shown in Fig. 4 (F to J), although Clotrimazole had a strong anti–*C. albicans* activity toward clinical isolates, it had severe cytotoxicity at very low concentrations (fig. S22); on the other hand, it could not adjust the pH of MRS medium (fig. S20). Therefore, if Clotrimazole was used to treat *C. albicans*–infected vaginitis, then it would not only affect the repair of vaginal mucosa but also increase the risk of *Candida* vaginitis recurrence due to failure to regulate the vaginal microenvironment.

Effects of rGO@FeS_2 nanozyme oxidation on their activities

It is critical to maintain the anti–*C. albicans* and POD-like activities of rGO@FeS_2 for *Candida* vaginitis therapy. We investigated the sensitivity of rGO@FeS_2 to oxygen by storing the material in vacuum and air for 12 days via XRD and XPS analysis. As shown in fig. S23, rGO@FeS_2 nanozymes were oxidized when exposed to air, whereas their oxidation was obviously reduced in vacuum. We further monitored the anti–*C. albicans* activity of rGO@FeS_2 after potential oxidation. It was shown that the anti–*C. albicans* activity of rGO@FeS_2 exposed to air gradually decreased (fig. S24, A to C) and disappeared after 12 days (fig. S24D) in the presence of H_2O_2. In contrast, rGO@FeS_2 with H_2O_2 retained the anti–*C. albicans* activity after 30 days of storage in vacuum (fig. S24E). Accordingly, the $^{\bullet}OH$ generating activity of oxidized rGO@FeS_2 and H_2O_2 was notably reduced (fig. S24F). Notably, although rGO@FeS_2 nanozymes were sensitive to oxygen and the potential oxidation can affect their anti–*C. albicans* and POD-like activities, the proper storage would retain the activities. In practice, medications can be vacuum packed to prolong the storage time. In our study, we developed a hydrogel formulation of rGO@FeS_2 and *Lactobacillus*, which will be easily vacuum-packed. We therefore reason that the activities of rGO@FeS_2 would be effectively retained for practical use, for example, using vacuum packaging.

Effects of FeLab on *C. albicans* and *Lactobacillus* and the release profile of *Lactobacillus* with HAase in vitro

Since HAase secreted by *Candida* and bacteria can degrade HA, we used HA hydrogel to encapsulate rGO@FeS_2 nanozymes and *Lactobacillus* to form a FeLab preparation (*25*, *36*). It was beneficial to inject the hydrogel delivery system into the vagina and reduce leakage. Moreover, through the controllably triggered response to the *C. albicans*–infected microenvironment, the hydrogel preparation could achieve an enhanced ROS concentration in situ and minimize damage to vaginal mucosal cells (*37*). While having the above advantages, it was critical that the encapsulation within HA hydrogels neither affected the viability of *Lactobacillus* nor hindered anti–*C. albicans* effects exerted by the self-cascading reaction between rGO@FeS_2 nanozymes and *Lactobacillus*. As shown in fig. S25A, the viability of *Lactobacillus* (10^5 CFU/ml) encapsulated in HA hydrogels was not affected. Therefore, *Lactobacillus* (10^5 CFU/ml) was encapsulated into HA hydrogels for further anti–*C. albicans* activities. Compared with the treatment of other HA hydrogels [i.e., *Lactobacillus*@HA (Lab), rGO@HA, rGO@FeS_2@HA, and rGO/*Lactobacillus*@HA (rGOLab)], the pH of MRS medium could be lowered to around 4.5 after treatment with FeLab (fig. S25B). Moreover, the cell viability of *C. albicans* treated with FeLab was significantly decreased, confirming the retained antifungal activity of rGO@FeS_2/*Lactobacillus* after HA coating (fig. S25, C and D). Then, the HAase-simulated release profile of *Lactobacillus* was investigated. As shown in fig. S26, stimulated by the HAase solution, *Lactobacillus* showed a sustained release and achieved a nearly 100% release in 24 hours. In contrast, HA hydrogels without HAase solution did not cause substantial leakage of cargoes, indicating that the HA hydrogel with HAase secreted by *Candida* and bacteria can controllably release contents for anti–*C. albicans* activities.

Antifungal effects of FeLab on *C. albicans*–induced vaginitis in vivo

To further assess its potential as a topical antifungal medication, we evaluated the antifungal effects of FeLab on *C. albicans*–induced vaginitis in vivo. Clotrimazole group (as a representative small molecule drug) was included for comparison. First, female BALB/c mice were injected with estradiol benzoate solutions every 2 days. Then, *C. albicans* solutions were injected into the vagina to establish a vaginitis model of *C. albicans* infection. After successful establishment of the model, treatments were performed intravaginally once a day for 5 days. Last, vaginal washes were obtained for colony counting and microbiota composition analysis. Subsequently, mice were euthanized to obtain vaginal tissues for histochemistry (Fig. 5A). As shown in Fig. 5 (B and C) and fig. S27, compared with Lab treatment, the cell viability and colony formation of *C. albicans* with both FeLab and Clotrimazole treatments were significantly decreased in vaginal washes. Histochemistry analysis showed that main organs, including the heart, liver, spleen, lung, and kidney, were not affected after 5 days of continuous vaginal administration in all treatment groups (fig. S28). However, through histological staining of vaginal tissues, vaginal keratinization and mucosal and submucosal inflammatory cell infiltration in the FeLab treatment group were notably lower than those in the group treated with

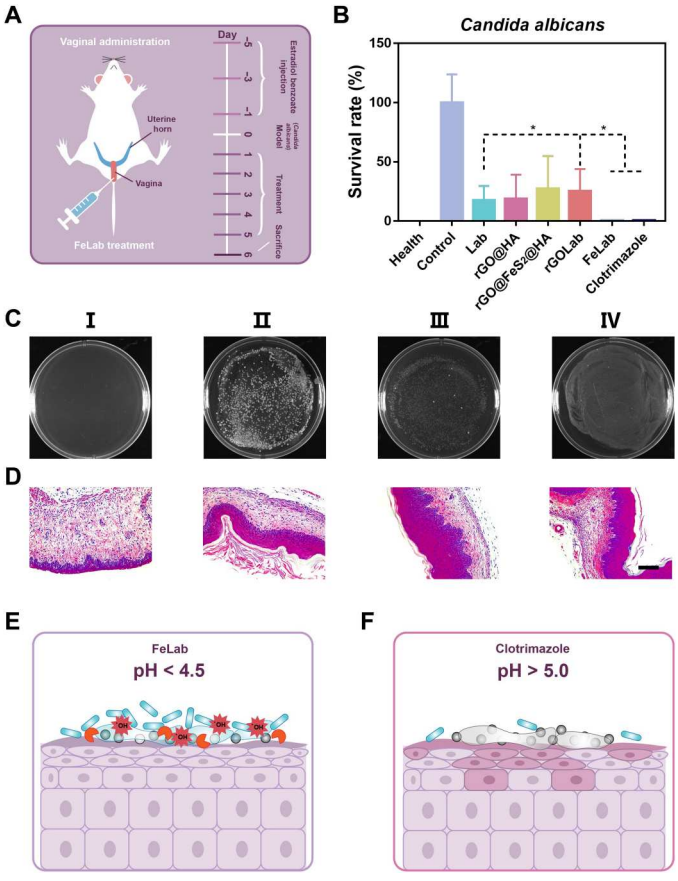

Fig. 5. Antifungal effects of FeLab on *C. albicans*–induced vaginitis in vivo. (**A**) Experimental scheme of *C. albicans*–infected vaginitis mice. (**B**) Cell viabilities of *C. albicans* in vaginal washes after indicated treatments. (**C** and **D**) Digital images of *C. albicans* colonies in the vaginal washes (C) and H&E-staining images of the vaginal tissue (D) in different groups. I, health; II, control; III, FeLab; IV, Clotrimazole. Scale bar, 100 μm. (**E** and **F**) Schematic diagram comparing FeLab (E) with Clotrimazole (F) for the treatment of *Candida* vaginitis in mice. Data are presented as means ± SD ($n = 5$). *$P < 0.05$.

Clotrimazole (Fig. 5D and fig. S29). This indicated that Clotrimazole caused serious damage to vaginal mucosa cells (consistent with the results of fig. S22), while FeLab was conducive to promoting the repair of vaginal mucosa. Together, the above results indicated that the responsive release of FeLab was triggered at the vaginal site infected with *C. albicans*. After release, *Lactobacillus* could regulate the microenvironment of the vagina by reducing the pH to about 4.5 and producing H_2O_2, which was conducive to the catalysis of rGO@FeS_2 nanozymes to generate a large amount of $^{\bullet}OH$ to kill *C. albicans* in situ, thereby minimizing the damage to vaginal mucosal cells (Fig. 5E) (*7*, *38*). In contrast, although Clotrimazole had anti–*C. albicans* activity by affecting the permeability of the cell membrane, it caused severe damage to vaginal mucosal cells due to poor selectivity. On the other hand, Clotrimazole could not regulate the pH of the vagina (over 5.0; fig. S20), which is the optimal condition for *C. albicans* to grow and may lead to a greater risk of *Candida* vaginitis recurrence than FeLab (Fig. 5F).

To test our hypothesis, we next investigated the effects of FeLab and Clotrimazole on *Candida* vaginitis recurrence in mice. *Candida* vaginitis mice in Fig. 5A were treated with FeLab and Clotrimazole, respectively. Then, *C. albicans* solutions were reinjected into the vagina to establish a recurrence model. After 24 hours, vaginal washes and vaginal tissues were collected to assess recurrence effects. As shown in fig. S30, the cell viability and colonies of *C. albicans* treated with FeLab were lower than those treated with Clotrimazole in vaginal washes. Moreover, the hematoxylin and eosin (H&E) analysis of vaginal tissues revealed that the former had less infiltration of vaginal mucositis cells. These results suggested that although Clotrimazole had strong anti–*C. albicans* activity, FeLab could more notably reduce the risk of *Candida* vaginitis recurrence (*3*).

Vaginal microbiome amelioration in mice with *C. albicans*–induced vaginitis after FeLab treatment versus Clotrimazole

Evidence suggests that patients with *Candida* vaginitis are associated with dysbiosis characterized by decreased biodiversity, a lower proportion of the *Firmicutes* ratio, and an increase in *Proteobacteria* (*39*, *40*). Thus, we investigated whether FeLab therapy could better modulate the composition of the vaginal microbiota than Clotrimazole treatment in mice through the second ribosomal internal transcribed spacer amplicon sequencing and the Sobs and Shannon entropy index of α-diversity by 16S ribosomal RNA gene sequencing. Analysis of vaginal wash samples revealed that compared with Clotrimazole, FeLab treatment markedly improved fungal and bacterial diversities in mice with *Candida* vaginitis, as indicated by the increase in the number of unique operational taxonomic units (Fig. 6, A and B, and fig. S31). Further analysis at the phylum level revealed that FeLab treatment markedly reduced the relative abundance of *Proteobacteria* and increased the relative abundance of *Firmicutes*, reshaping a healthier vaginal microbiome (Fig. 6, C to E). At the genus level, the relative abundance of *Lactobacillus*, which can promote the maintenance of vaginal homeostasis and prevent the colonization and growth of adverse microorganisms, significantly increased (Fig. 6F and fig. S32), while *Proteus* significantly decreased (Fig. 6G) after treatment with FeLab (*41*–*43*). Together, compared with Clotrimazole, FeLab could increase the richness and diversity of the vaginal microbiome, especially *Lactobacillus*, to efficiently treat *Candida* vaginitis and reduce the recurrence, demonstrating the promise to treat and prevent vaginal dysbiosis. We are also aware that the vaginal microenvironment and microbiota of rodent models are different from those of humans in *Candida* vaginitis (*44*, *45*). Therefore, a detailed relationship between rodent models and human disease still needs further exploration.

DISCUSSION

In summary, a responsive hydrogel FeLab with POD-like and vaginal microenvironment regulating activities was developed to kill *C. albicans* and modulate vaginal microbiota balance for *Candida* vaginitis treatment and reduce the recurrence. The designed rGO@FeS_2 structure ensured uniform dispersion of marcasite FeS_2 nanoparticles on the rGO supports, and the encapsulated *Lactobacillus* could produce H_2O_2 and lower the pH, facilitating the enhancement of POD-like activity to kill *C. albicans* in a *C. albicans*–induced vaginitis model. The self-cascade catalysis hardly affected *Lactobacillus*, thus effectively improving vaginal microbiota and reshaping a healthier vaginal microenvironment. This work not only demonstrates the advantages of nanozyme-probiotic

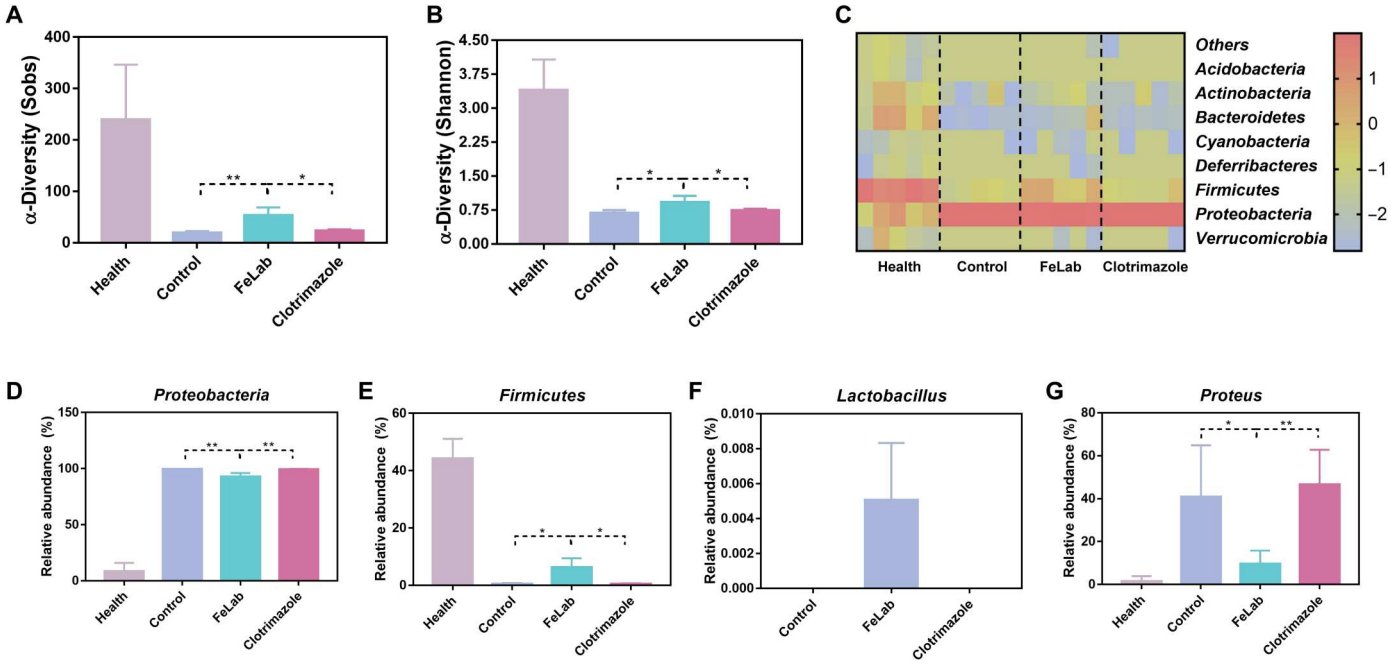

Fig. 6. Vaginal microbiome amelioration in mice with *C. albicans*–induced vaginitis after FeLab treatment versus Clotrimazole. (**A** and **B**) α-Diversity Sobs (A) and Shannon (B) indexes of the vaginal microbiome. (**C**) Heatmap of the relative abundance of phylum-level taxa for each mouse (columns). (**D** and **E**) Relative abundance of *Proteobacteria* (D) and *Firmicutes* (E) taxa, respectively. (**F** and **G**) Relative abundance of genus-level taxa for *Lactobacillus* (F) and *Proteus* (G), respectively. Data are presented as means ± SD (n = 4). *P < 0.05 and **P < 0.01.

combinations over small molecular antifungal drugs for *Candida* vaginitis treatment and reducing recurrence but also shows the translational promise of nanozymes.

MATERIALS AND METHODS

Materials

Iron chloride hexahydrate ($FeCl_3{\cdot}6H_2O$), ferrous sulfate ($FeSO_4$), ferric chloride ($FeCl_3$), thiourea [$(NH_2)_2CS$], sodium hydroxide (NaOH), hydrochloric acid (HCl), hydrogen peroxide (H_2O_2; 30%), benzoic acid, NaAc, ethylene glycol (EG), trichloromethane ($CHCl_3$), and ammonia water ($NH_3{\cdot}H_2O$; 25 to 28%) were purchased from Sinopharm Chemical Reagent Co. Ltd. (Shanghai, China). Polyvinylpyrrolidone (PVP; 8000) and TMB were purchased from Aladdin Chemical Co. Ltd. (Shanghai, China). Iron acetylacetonate [$Fe(acac)_3$] and platinum acetylacetonate [$Pt(acac)_2$] were purchased from J&K Scientific Co. Ltd. (Beijing, China). Sodium hyaluronic acid (weight-average molecular weight = 0.3 MDa), HAase, L-cysteine methyl ester hydrochloride, 1-ethyl-3-(3-dimethylaminopropyl)carbodiimide hydrochloride (EDC), and *N*-hydroxysuccinimide (NHS) were purchased from Yuanye Bio-Technology Co. Ltd. (Shanghai, China). DMPO was purchased from JK Chemical and Dojindo (Japan). Dimethyl sulfoxide (DMSO), DCFH-DA, PI, methylthiazolyldiphenyl-tetrazolium bromide (MTT), and Dulbecco's modified Eagle medium (DMEM) were purchased from Beyotime Chemical Reagent Co. Ltd. (Shanghai, China). FilmTracer FM 1-43 was purchased from Thermo Fisher Scientific (USA). MRS medium was obtained from Haibo Biotechnology Co. Ltd. (Shandong, China). Estradiol benzoate injection was purchased from Quanyu Bio-Technology Animal Pharmaceutical Co. Ltd. (Shanghai, China). Clotrimazole suppository was purchased from Baiyunshan Pharmaceutical Holdings Co. Ltd. (Guangdong, China). GO was purchased from Jiangsu Xianfeng Nanomaterials Technology Co. Ltd. (Jiangsu, China). All aqueous solutions were prepared with deionized water (18.2 megohm·cm; Millipore).

Instrumentation

TEM imaging was performed on a JEM-2100 (JEOL, Japan) transmission electron microscope at an acceleration voltage of 200 kV. Powder XRD patterns were measured at 5°/min using a diffractometer (Rigaku Ultima III, Japan and Bruker D8 advance, Germany) with a Cu Kα radiation. XPS spectra were collected by using a PHI 5000 Versa Probe XPS microscope (Ulvac-Phi, Japan). Ultraviolet-visible absorption spectra were measured on a SpectraMax M2e microplate reader (Molecular Devices, USA). HAADF-STEM and the corresponding energy-dispersive spectroscopy elemental mappings were performed on a Tecnai G2 F30 (FEI, USA). EPR spectra were recorded on a Bruker A300 spectrometer (X-band). The pH value of MRS medium was measured using a pH meter (STARTER 3100, USA). Cell images of *C. albicans* and *Lactobacillus* were recorded on a laser scanning confocal microscope (Olympus, Japan). Tissue images of H&E staining were photographed by a DMi8 fluorescence microscope (Leica, Germany).

Synthesis of rGO@FeS_2, Pt_3Fe, Fe_3O_4, and pyrite FeS_2 nanozymes

rGO@FeS_2 nanozymes were synthesized as follows (*34*). Five milliliters of $FeCl_3$ (0.135 g/ml), 5 ml of $(NH_2)_2CS$ (0.038 g/ml), and 30 μl of $NH_3{\cdot}H_2O$ were added to 7.5 ml of GO aqueous solution (5.6

mg/ml) under mild ultrasonication. Subsequently, the mixture solution was heated at 180°C for 12 hours to form marcasite FeS_2 nanoparticle–decorated rGO (rGO@FeS_2). After rGO@FeS_2 nanozymes were dialyzed with ultrapure water for 3 days, they were subjected to lyophilization for use. For comparison, rGO supports and pristine marcasite FeS_2 nanoparticles were also prepared via similar methods without the addition of $FeCl_3$ and $(NH_2)_2CS$ or GO aqueous solutions, respectively.

Pt_3Fe nanozymes were synthesized as follows (*28*). $Pt(acac)_2$ (20.21 mg), $Fe(acac)_3$ (21.4 mg), benzoic acid (50 mg), and PVP (80 mg) were dispersed in benzyl alcohol (5 ml) under vigorous stirring for 15 min. Subsequently, the resultant mixture was transferred into a reactor at 180°C for 12 hours. Pt_3Fe nanozymes were precipitated by acetone, washed six times with an ethanol-acetone mixture, and dispersed into water for use.

Fe_3O_4 nanozymes were synthesized as follows (*29*). A mixture of $FeCl_3$ and $FeSO_4$ (molar ratio, 2:1) solutions was prepared under N_2 protection. Then, enough $NH_3{\cdot}H_2O$ was dropped into it under vigorous stirring. After 30 min, the resulting Fe_3O_4 nanozymes were washed five times immediately with distilled water by magnetic separation.

Pyrite FeS_2 nanozymes were synthesized as follows (*30*). Since the as-synthesized marcasite FeS_2 nanoparticles were too compacted to disperse (Fig. 2C), we synthesized pyrite FeS_2 nanozymes for comparison. In a typical synthesis, PVP (0.7 g), $FeCl_3{\cdot}6H_2O$ (0.5 g), and NaAc (3.6 g) were dispersed into 30 ml of EG solution under vigorous stirring. Next, S powder (0.4 g) was added, and the resultant mixture was ultrasonicated for 1 hour to form a homogeneous dispersion. The mixture was transferred into a reactor at 200°C for 12 hours. Pyrite FeS_2 nanozymes were isolated with the addition of excess $CHCl_3$, alcohol, and ultrapure water by centrifugation.

Synthesis of HA hydrogel

The HA hydrogel was prepared following a previously reported method (*37*). In detail, HA (0.4 g), NHS (0.575 g, 5 mM), and EDC (0.958 g, 5 mM) were dissolved thoroughly in deionized water (100 ml) for 1 hour at room temperature to fully activate the carboxylic groups of HA. Then, L-cysteine methyl ester hydrochloride (0.855 g, 5 mM) was added to the mixture under continuous stirring for 24 hours with light protection. The pH value of the above solution was adjusted to 4.8 by adding 1.0 M NaOH or 1.0 M HCl. The resulting solution was dialyzed (molecular weight cutoff, 1000) against dilute HCl solution (pH 3.5) to remove unnecessary agents, followed by lyophilization to obtain the target conjugates as fluffy solids (HA-SH). Then, HA-SH conjugates (16 mg), *Lactobacillus* (10^5 CFU/ml), and rGO@FeS_2 nanozymes (25 μg/ml) were dissolved in phosphate-buffered saline (PBS) (400 μl; pH 8), and the mixture was vortexed for 10 s to yield a homogeneous stock solution. After that, the precursor solution was incubated at 37°C without shaking for complete FeLab formation. Similarly, a series of hydrogels with/without *Lactobacillus* or rGO@FeS_2 nanozymes were prepared.

POD-like activity and kinetic assay

The POD-like activity of rGO@FeS_2 nanozymes was determined using TMB as the substrate in the presence of H_2O_2. In a typical experiment, rGO@FeS_2 nanozymes (25 μg/ml), TMB (0.2 mM), and H_2O_2 (0.08 mM) were added to 200 μl of HAc-NaAc buffer (0.1 M; pH 4.5). Then, the absorbance at 652 nm for oxTMB was recorded at a certain reaction time to evaluate the POD-like activity. The pH-dependent POD-like activity of rGO@FeS_2 nanozymes was studied under different pH values, including 4.0, 4.5, 5.0, 5.5, 6.0, and 6.5, in HAc-NaAc buffer.

Steady-state kinetics assays were conducted at 25°C in 200 μl of HAc-NaAc buffer with rGO@FeS_2 nanozymes (25 μg/ml) as a catalyst in the presence of H_2O_2 and TMB. On the one hand, TMB (0.2 mM) and different concentrations of H_2O_2 (0, 0.025, 0.05, 0.1, 0.2, 0.4, and 0.8 mM) were added to the reaction system with H_2O_2 as the substrate. On the other hand, H_2O_2 (0.08 mM) and different concentrations of TMB (0, 0.1, 0.2, 0.3, 0.35, 0.4, and 0.45 mM) were added to the reaction system with TMB as the substrate. The Michaelis-Menten constants were calculated according to the Michaelis-Menten saturation curve by GraphPad Prism 7.0 (GraphPad Software).

Lactobacillus and *C. albicans* culture

Lactobacillus capsules (S20030005) for treating bacterial vaginitis were obtained from Inner Mongolia Shuangqi Pharmaceutical Co. Ltd. The capsules were dissolved in MRS medium and inoculated on MRS medium agar plates for 12 hours (microaerophilic conditions at 37°C) via an inoculation loop to obtain a single colony. The single colony was placed in fresh MRS medium and cultured overnight for further experiments. *C. albicans*, including five samples of clinical isolates, was cultured in a similar method except under microaerophilic conditions.

Anti–*C. albicans* activities of four nanozymes

C. albicans cultures were washed three times with sterile PBS and divided into twelve groups: (i) control (*C. albicans*), (ii) *C. albicans* + H_2O_2, (iii) *C. albicans* + rGO, (iv) *C. albicans* + rGO@FeS_2, (v) *C. albicans* + Pt_3Fe, (vi) *C. albicans* + Fe_3O_4, (vii) *C. albicans* + pyrite, (viii) *C. albicans* + rGO + H_2O_2, (ix) *C. albicans* + rGO@FeS_2 + H_2O_2, (x) *C. albicans* + Pt_3Fe + H_2O_2, (xi) *C. albicans* + Fe_3O_4 + H_2O_2, and (xii) *C. albicans* + pyrite + H_2O_2. The concentrations of *C. albicans*, H_2O_2, and nanozymes were 10^6 CFU/ml, 80 μM, and 25 μg/ml in HAc-NaAc buffer (0.1 M; pH 5.0), respectively. These mixed suspensions were then incubated for 2 hours at 37°C, and 100 μl from them was spread evenly on MRS medium agar plates. After incubation for 48 hours at 37°C, the photos were taken, and quantitative analysis of anti–*C. albicans* activities was performed by ImageJ.

Electron spin resonance analysis of $^{\bullet}OH$ formation

Glass capillary tubes containing four nanozymes (25 μg/ml), H_2O_2 (80 μM), DMPO (10 mM), and HAc-NaAc buffer (0.1 M; pH 4.5) were inserted into the EPR cavity to record $^{\bullet}OH$ signals after 5 min of reaction.

Enhanced anti–*C. albicans* activities with *Lactobacillus*, including five samples of clinical isolates in vitro

Five samples of clinically isolated *C. albicans* were obtained from the Department of Clinical Laboratory of Nanjing Drum Tower Hospital, Medical School of Nanjing University of consent and processed with approval from the Review Board (2022-543-01). *C. albicans* and *Lactobacillus* cultured were washed three times with sterile PBS and divided into seven groups in a 24-well plate: (i) control (*C. albicans*), (ii) *C. albicans* + *Lactobacillus*, (iii) *C. albicans* + rGO, (iv) *C. albicans* + rGO@FeS_2, (v) *C. albicans* + rGO +

Lactobacillus, (vi) *C. albicans* + rGO@FeS_2 + *Lactobacillus*, and (vii) *C. albicans* + Clotrimazole. The final concentrations of *C. albicans*, *Lactobacillus*, rGO@FeS_2, and Clotrimazole were 10^6 CFU/ml, 10^2 CFU/ml, 25 μg/ml, and 25 μg/ml (except excipient), respectively, in 2 ml of MRS medium. These mixed suspensions were then incubated for 24 hours at 37°C under microaerophilic conditions, and 100 μl of them was spread on MRS medium agar plates. After incubation for 48 hours under the same culture conditions, the photos were taken, and the quantitative analysis of anti–*C. albicans* activities was performed by ImageJ. *C. albicans* formed large and milky colonies, whereas *Lactobacillus* was small and transparent. In addition, the pH values of the mixed MRS medium were measured with a pH meter.

Determination of intracellular ROS

As an oxidant-sensitive dye, DCFH-DA was used to measure intracellular ROS levels. *C. albicans*, *Lactobacillus*, or a mixture of both were stained with 10 μM DCFH-DA for 30 min in the dark at room temperature and washed twice with sterile PBS, followed by (i) to (vi) treatments. The intracellular ROS levels were measured using a confocal laser microscope with excitation and emission wavelengths at 488 and 525 nm, respectively.

Morphological observation of *C. albicans* and *Lactobacillus*

Nest circle microscope cover glass was used at the bottom of a 24-well plate. The *C. albicans* and *Lactobacillus* treated by (i) to (vii) for 24 hours were fixed with 2.5% glutaraldehyde overnight at 4°C in the dark. The fungal and bacterial cells were then dehydrated with 30, 50, 70, 80, 90, and 100% of ethanol, respectively, for 10 min. Last, the dried cells were sputter-coated with iridium (6 nm) for SEM observation.

Live/dead cell staining of *C. albicans* and *Lactobacillus*

The *C. albicans* and *Lactobacillus* treated by (i) to (vi) were stained with FilmTracer FM 1-43 and PI for 30 min and washed three times with sterile 0.9% NaCl solution for visualization via a confocal fluorescence microscope.

In vitro cytotoxicity experiments

The cell viabilities of mouse embryonic fibroblast cells (NIH/3T3) and a human normal hepatocyte line (L02) to rGO, rGO@FeS_2, and Clotrimazole were determined by an MTT assay. First, the cells were incubated with DMEM in a 96-well plate (about 5000 cells per well, five wells per concentration) in a humidified incubator (37°C, 5% CO_2) for 24 hours. Then, the cells were treated with different concentrations of rGO, rGO@FeS_2, and Clotrimazole solutions (10, 25, 50, 80, and 100 μg/ml) for 12 hours. Subsequently, MTT (0.5 mg/ml) was added to the cells and incubated for 4 hours. Last, the medium was removed, and 100 μl of DMSO was added. The absorbance was determined at 490 nm, and the cell viabilities were expressed as a percentage of the control.

Controlled-release experiment of *Lactobacillus*

The release behavior of *Lactobacillus* from HA hydrogels was monitored as follows (*37*). A certain amount of *Lactobacillus* was encapsulated in a hydrogel of 10^9 CFU/ml. Specifically, the prepared Lab (10 ml) was individually immersed into PBS buffer (50 ml; pH 5.0) and HAase solution (150 U/mg) with constant shaking. At predetermined time intervals, 100 μl of the surrounding medium was taken to measure the optical density at 600 nm by a microplate reader. The release rate was calculated on the basis of the percentage of released *Lactobacillus* within the whole encapsulated *Lactobacillus* in the respective release medium.

C. albicans–infected vaginitis model and therapeutic process in vivo

All animal experiments were approved by the Committee for Experimental Animals Welfare and Ethics of Nanjing University (Institutional Animal Care and Use Committee, 2202010). The anti–*C. albicans* effects of FeLab were evaluated by using *C. albicans*–infected mice. After 7 days of adaptation to the environment, female BALB/c mice (18 to 20 g) were randomly divided into eight groups with six mice per group: (i) health, (ii) control, (iii) Lab, (iv) rGO@HA, (v) rGO@FeS_2@HA, (vi) rGOLab, (vii) FeLab, and (viii) Clotrimazole. Mice except the healthy group were subcutaneously injected with 0.1 ml of estradiol benzoate injection (2 mg/ml) once 2 days for 6 days. On the 7th day, 20 μl of *C. albicans* solution (1×10^9 CFU/ml) was injected into the vagina with a pipette gun, and the mice were fed normally for 1 day. Note that this day was designated as day 0. *C. albicans*–induced mice were intravaginally injected with various HA hydrogels (4%) and Clotrimazole for five consecutive days (days 1, 2, 3, 4, and 5). Among them, the concentrations of encapsulated *Lactobacillus*, rGO@FeS_2, and Clotrimazole were 10^5 CFU/ml, 0.4 mg/kg, and 0.4 mg/kg (except excipient), respectively. On day 6, the vagina was washed repeatedly with sterile PBS (20 μl) by pipetting five times to obtain vaginal washes, which were used for quantitative analysis of *C. albicans* cell viability on MRS medium agar plates and vaginal microbiome analysis. Following anesthesia with diethyl ether, all groups of mice were euthanized, and the vagina, heart, liver, spleen, lung, and kidney were collected and fixed with paraformaldehyde (4%). These tissues were dissected, analyzed by H&E staining, and imaged by an optical microscope.

C. albicans–infected vaginitis recurrence model in vivo

On the basis of the above modeling methods, 12 *C. albicans*–infected mice were equally divided into two groups and then treated with FeLab and Clotrimazole, respectively. Note that this day was designated as day 0. On day 1, 20 μl of *C. albicans* solution (1×10^9 CFU/ml) was injected into the vagina with a pipette gun, and the mice were fed normally for 1 day. Similarly, vaginal washes were obtained for quantitative analysis of *C. albicans* cell viability, and vaginal tissues were collected for further H&E analysis.

Statistical analysis

Data were shown as means ± SD. Statistical analysis was performed using Student's *t* test for two-group differences and one-way two-sided analysis of variance (ANOVA) for multiple comparisons. $^*P < 0.05$, $^{**}P < 0.01$, $^{***}P < 0.001$, and $^{****}P < 0.0001$

Supplementary Materials

This PDF file includes:

Figs. S1 to S32
Table S1

REFERENCES AND NOTES

1. M. Ilkit, A. B. Guzel, The epidemiology, pathogenesis, and diagnosis of vulvovaginal candidosis: A mycological perspective. *Crit. Rev. Microbiol.* **37**, 250–261 (2011).
2. L. O. Eckert, Acute vulvovaginitis. *N. Engl. J. Med.* **355**, 1244–1252 (2006).
3. D. W. Denning, M. Kneale, J. D. Sobel, R. Rautemaa-Richardson, Global burden of recurrent vulvovaginal candidiasis: A systematic review. *Lancet Infect. Dis.* **18**, e339–e347 (2018).
4. Å. Sullivan, C. Edlund, C. E. Nord, Effect of antimicrobial agents on the ecological balance of human microflora. *Lancet Infect. Dis.* **1**, 101–114 (2001).
5. S. L. Hillier, M. A. Krohn, L. K. Rabe, S. J. Klebanoff, D. A. Eschenbach, The normal vaginal flora, H_2O_2-producing *Lactobacilli*, and bacterial vaginosis in pregnant women. *Clin. Infect. Dis.* **16**, 273–281 (1993).
6. J. M. Wells, A. Mercenier, Mucosal delivery of therapeutic and prophylactic molecules using lactic acid bacteria. *Nat. Rev. Microbiol.* **6**, 349–362 (2008).
7. M. France, M. Alizadeh, S. Brown, B. Ma, J. Ravel, Towards a deeper understanding of the vaginal microbiota. *Nat. Microbiol.* **7**, 367–378 (2022).
8. S. Husain, J. Allotey, Z. Drymoussi, M. Wilks, B. M. Fernandez-Felix, A. Whiley, J. Dodds, S. Thangaratinam, C. McCourt, E. M. Prosdocimi, W. G. Wade, B. M. de Tejada, J. Zamora, K. Khan, M. Millar, Effects of oral probiotic supplements on vaginal microbiota during pregnancy: A randomised, double-blind, placebo-controlled trial with microbiome analysis. *BJOG* **127**, 275–284 (2020).
9. J. van de Wijgert, M. C. Verwijs, *Lactobacilli*-containing vaginal probiotics to cure or prevent bacterial or fungal vaginal dysbiosis: A systematic review and recommendations for future trial designs. *BJOG* **127**, 287–299 (2020).
10. Y. Lee, E. Puumala, N. Robbins, L. E. Cowen, Antifungal drug resistance: Molecular mechanisms in *Candida albicans* and beyond. *Chem. Rev.* **121**, 3390–3411 (2021).
11. J. Berman, P. E. Sudbery, *Candida albicans*: A molecular revolution built on lessons from budding yeast. *Nat. Rev. Genet.* **3**, 918–931 (2002).
12. M. C. Watson, J. M. Grimshaw, C. M. Bond, J. Mollison, A. Ludbrook, Oral versus intra-vaginal imidazole and triazole anti-fungal agents for the treatment of uncomplicated vulvovaginal candidiasis (thrush): A systematic review. *BJOG* **109**, 85–95 (2002).
13. C. M. A. Santos, M. C. V. Pires, T. L. Leão, Z. P. Hernández, M. L. Rodriguez, A. K. S. Martins, L. S. Miranda, F. S. Martins, J. R. Nicoli, Selection of *Lactobacillus* strains as potential probiotics for vaginitis treatment. *Microbiology* **162**, 1195–1207 (2016).
14. R. Palmeira-de-Oliveira, A. Palmeira-de-Oliveira, J. Martinez-de-Oliveira, New strategies for local treatment of vaginal infections. *Adv. Drug. Deliver. Rev.* **92**, 105–122 (2015).
15. M. Pirotta, J. Gunn, P. Chondros, S. Grover, P. O'Malley, S. Hurley, S. Garland, Effect of *lactobacillus* in preventing post-antibiotic vulvovaginal candidiasis: A randomised controlled trial. *BMJ* **329**, 548–553 (2004).
16. R. Alonso-Roman, A. Last, M. H. Mirhakkak, J. L. Sprague, L. Möller, P. Großmann, K. Graf, R. Gratz, S. Mogavero, S. Vylkova, G. Panagiotou, S. Schäuble, B. Hube, M. S. Gresnigt, *Lactobacillus rhamnosus* colonisation antagonizes *Candida albicans* by forcing metabolic adaptations that compromise pathogenicity. *Nat. Commun.* **13**, 3192–3207 (2022).
17. M. E. Falagas, G. I. Betsi, S. Athanasiou, Probiotics for the treatment of women with bacterial vaginosis. *Clin. Microbiol. Infect.* **13**, 657–664 (2007).
18. E. Brillas, I. Sirés, M. A. Oturan, Electro-Fenton process and related electrochemical technologies based on Fenton's reaction chemistry. *Chem. Rev.* **109**, 6570–6631 (2009).
19. A. Scheeline, D. L. Olson, E. P. Williksen, G. A. Horras, M. L. Klein, R. Larter, The peroxidase-oxidase oscillator and its constituent chemistries. *Chem. Rev.* **97**, 739–756 (1997).
20. L. Zhang, S.-S. Wan, C.-X. Li, L. Xu, H. Cheng, X.-Z. Zhang, An adenosine triphosphate-responsive autocatalytic Fenton nanoparticle for tumor ablation with self-supplied H_2O_2 and acceleration of Fe(III)/Fe(II) conversion. *Nano Lett.* **18**, 7609–7618 (2018).
21. L. Gao, J. Zhuang, L. Nie, J. Zhang, Y. Zhang, N. Gu, T. Wang, J. Feng, D. Yang, S. Perrett, X. Yan, Intrinsic peroxidase-like activity of ferromagnetic nanoparticles. *Nat. Nanotechnol.* **2**, 577–583 (2007).
22. J. Wu, X. Wang, Q. Wang, Z. Lou, S. Li, Y. Zhu, L. Qin, H. Wei, Nanomaterials with enzyme-like characteristics (nanozymes): Next-generation artificial enzymes (II). *Chem. Soc. Rev.* **48**, 1004–1076 (2019).
23. B. Yang, Y. Chen, J. Shi, Reactive oxygen species (ROS)-based nanomedicine. *Chem. Rev.* **119**, 4881–4985 (2019).
24. M. Liu, L. Huang, X. Xu, X. Wei, X. Yang, X. Li, B. Wang, Y. Xu, L. Li, Z. Yang, Copper doped carbon dots for addressing bacterial biofilm formation, wound infection, and tooth staining. *ACS Nano* **16**, 9479–9497 (2022).
25. R. Stern, M. J. Jedrzejas, Hyaluronidases: Their genomics, structures, and mechanisms of action. *Chem. Rev.* **106**, 818–839 (2006).
26. M. S. Kim, S. Cho, S. H. Joo, J. Lee, S. K. Kwak, M. I. Kim, J. Lee, N- and B-codoped graphene: A strong candidate to replace natural peroxidase in sensitive and selective bioassays. *ACS Nano* **13**, 4312–4321 (2019).
27. M. S. Kim, J. Lee, H. S. Kim, A. Cho, K. H. Shim, T. N. Le, S. S. A. An, J. W. Han, M. I. Kim, J. Lee, Heme cofactor-resembling fe-n single site embedded graphene as nanozymes to selectively detect H_2O_2 with high sensitivity. *Adv. Funct. Mater.* **30**, 5410–5420 (2019).
28. Z. Wang, Y. Zhang, E. Ju, Z. Liu, F. Cao, Z. Chen, J. Ren, X. Qu, Biomimetic nanoflowers by self-assembly of nanozymes to induce intracellular oxidative damage against hypoxic tumors. *Nat. Commun.* **9**, 3334–3348 (2018).
29. Z. Chen, J.-J. Yin, Y.-T. Zhou, Y. Zhang, L. Song, M. Song, S. Hu, N. Gu, Dual enzyme-like activities of iron oxide nanoparticles and their implication for diminishing cytotoxicity. *ACS Nano* **6**, 4001–4012 (2012).
30. X. Meng, D. Li, L. Chen, H. He, Q. Wang, C. Hong, J. He, X. Gao, Y. Yang, B. Jiang, G. Nie, X. Yan, L. Gao, K. Fan, High-performance self-cascade pyrite nanozymes for apoptosis-ferroptosis synergistic tumor therapy. *ACS Nano* **15**, 5735–5751 (2021).
31. C.-H. Lai, M.-Y. Lu, L.-J. Chen, Metal sulfide nanostructures: Synthesis, properties and applications in energy conversion and storage. *J. Mater. Chem.* **22**, 19–30 (2012).
32. X. Du, I. Skachko, A. Barker, E. Y. Andrei, Approaching ballistic transport in suspended graphene. *Nat. Nanotechnol.* **3**, 491–495 (2008).
33. K. Han, W. Zhao, Q. Yu, Z. Liu, P. Li, W. Wang, L. Song, F. An, P. Cao, X. Qu, Marcasite-FeS_2@carbon nanodots anchored on 3D cell-like graphenic matrix for high-rate and ultrastable potassium ion storage. *J. Power Sources* **469**, 228429–228441 (2020).
34. R. Wang, M. Yan, H. Li, L. Zhang, B. Peng, J. Sun, D. Liu, S. Liu, FeS_2 nanoparticles decorated graphene as microbial-fuel-cell anode achieving high power density. *Adv. Mater.* **30**, 618–625 (2018).
35. H. Han, K. M. Kim, H. Choi, G. Ali, K. Y. Chung, Y.-R. Hong, J. Choi, J. Kwon, S. W. Lee, J. W. Lee, J. H. Ryu, T. Song, S. Mhin, Parallelized reaction pathway and stronger internal band bending by partial oxidation of metal sulfide-graphene composites: Important factors of synergistic oxygen evolution reaction enhancement. *ACS Catal.* **8**, 4091–4102 (2018).
36. R. Tian, X. Qiu, P. Yuan, K. Lei, L. Wang, Y. Bai, S. Liu, X. Chen, Fabrication of self-healing hydrogels with on-demand antimicrobial activity and sustained biomolecule release for infected skin regeneration. *ACS Appl. Mater. Interfaces* **10**, 17018–17027 (2018).
37. Y. Xiao, C. Lu, Y. Liu, L. Kong, H. Bai, H. Mu, Z. Li, H. Geng, J. Duan, Encapsulation of *Lactobacillus rhamnosus* in hyaluronic acid-based hydrogel for pathogen-targeted delivery to ameliorate enteritis. *ACS Appl. Mater. Interfaces* **12**, 36967–36977 (2020).
38. A. Lin, Y. Liu, X. Zhu, X. Chen, J. Liu, Y. Zhou, X. Qin, J. Liu, Bacteria-responsive biomimetic selenium nanosystem for multidrug-resistant bacterial infection detection and inhibition. *ACS Nano* **13**, 13965–13984 (2019).
39. B. J. Callahan, D. B. DiGiulio, D. S. A. Goltsman, C. L. Sun, E. K. Costello, P. Jeganathan, J. R. Biggio, R. J. Wong, M. L. Druzin, G. M. Shaw, D. K. Stevenson, S. P. Holmes, D. A. Relman, Replication and refinement of a vaginal microbial signature of preterm birth in two racially distinct cohorts of US women. *Proc. Natl. Acad. Sci. U.S.A.* **114**, 9966–9971 (2017).
40. J. Ravel, P. Gajer, Z. Abdo, G. M. Schneider, S. S. Koenig, S. L. McCulle, S. Karlebach, R. Gorle, J. Russell, C. O. Tacket, R. M. Brotman, C. C. Davis, K. Ault, L. Peralta, L. J. Forney, Vaginal microbiome of reproductive-age women. *Proc. Natl. Acad. Sci. U.S.A.* **108**, 4680–4687 (2011).
41. Human Microbiome Project Consortium, Structure, function and diversity of the healthy human microbiome. *Nature* **486**, 207–214 (2012).
42. P. Gajer, R. M. Brotman, G. Bai, J. Sakamoto, U. M. E. Schütte, X. Zhong, S. S. K. Koenig, L. Fu, Z. Ma, X. Zhou, Z. Abdo, L. J. Forney, J. Ravel, Temporal dynamics of the human vaginal microbiota. *Sci. Transl. Med.* **4**, 132–152 (2012).
43. M. N. Anahtar, D. B. Gootenberg, C. M. Mitchell, D. S. Kwon, Cervicovaginal microbiota and reproductive health: The virtue of simplicity. *Cell Host Microbe* **23**, 159–168 (2018).
44. A. Cassone, D. Sobel Jack, Experimental models of vaginal candidiasis and their relevance to human candidiasis. *Infect. Immun.* **84**, 1255–1261 (2016).
45. S. P. Rosshart, J. Herz, B. G. Vassallo, A. Hunter, M. K. Wall, J. H. Badger, J. A. McCulloch, D. G. Anastasakis, A. A. Sarshad, I. Leonardi, N. Collins, J. A. Blatter, S.-J. Han, S. Tamoutounour, S. Potapova, M. B. F. S. Claire, W. Yuan, S. K. Sen, M. S. Dreier, B. Hild, M. Hafner, D. Wang, I. D. Iliev, Y. Belkaid, G. Trinchieri, B. Rehermann, Laboratory mice born to wild mice have natural microbiota and model human immune responses. *Science* **365**, 4361–4390 (2019).

Acknowledgments

Funding: This work was supported by the National Key R&D Program of China (2019YFA0709200 and 2021YFF1200700), the National Natural Science Foundation of China (21874067 and 21722503), the CAS Interdisciplinary Innovation Team (JCTD-2020-08), the PAPD Program, and Fundamental Research Funds for the Central Universities (202200325). **Author contributions:** H.W. conceived the project. H.W. and G.W. designed the experiments. G.W., Q.L., W.L., Y.Z., X.Z., and W.Z. performed the experiments. G.W., Q.L., X.W., Z.Z., W.L., Y.Z., S.L., and C.Z. analyzed the results. H.W., G.W., X.W., Z.Z., W.L., and Y.Z. wrote the manuscript. All authors discussed the results and commented on the manuscript. **Competing interests:** The authors declare that they have no competing interests, and the patent application is in progress. **Data**

and materials availability: All data needed to evaluate the conclusions in the paper are present in the paper and/or the Supplementary Materials.

Submitted 1 December 2022
Accepted 14 April 2023
Published 17 May 2023
10.1126/sciadv.adg0949